Localization and Propagation of Instabilities in Long Shallow Panels Under External Pressure

T. L. Power

S. Kyriakides
Mem. ASME.

Engineering Mechanics Research Laboratory,
Department of Aerospace Engineering
and Engineering Mechanics,
The University of Texas at Austin,
Austin, TX 78712

This paper discusses the response of long, shallow, elastic panels to uniform pressure loading. Under quasi-static conditions, the deformation of such panels is initially uniform along their length, and their response has the nonlinearity and instabilities characteristic of shallow arches. Shallower panels deform symmetrically about the midspan and exhibit a limit load instability. For less shallow panels, the response bifurcates into an unsymmetric mode before the limit load is achieved. A formulation and a solution procedure are developed and used to analyze the response of such panels beyond first instability. It is demonstrated in both cases that following the first instability the deformation ceases to be axially uniform and localizes to a region a few arch spans in length. A drop in pressure accompanies this localized collapse and causes unloading in the remainder of the panel. Subsequent deformation is confined to this region until membrane tension arrests the local collapse. Further deformation can occur at a constant pressure and takes the form of spreading of the collapsed region along the length of the panel. The lowest pressure at which this can take place (propagation pressure) can be significantly lower than the pressure associated with first instability.

Introduction

This paper is concerned with the response and inherent instabilities in long, shallow, cylindrical panels under uniform pressure loading. Under quasi-static loading, the initial response of such panels has the nonlinearity and instabilities characteristic of shallow arches. Membrane deformations induced by the pressure cause a progressive softening of the response of the structure which for shallower panels results in a limit load instability (point *b* in the pressure-volume change response in Fig. 1(*a*)). For less shallow panels, this nonlinear response, which is symmetric about the midspan, is interrupted by a bifurcation-type instability. Consequently, the structure buckles into an unsymmetric mode before reaching the limit load (point *b* in Fig. 1(*b*)). In both types of panels the deformation remains axially uniform until the onset of the first instability. Our objective here is to explore the behavior of such panels beyond their first instability.

The response of arches (narrow strip rather than a long panel) beyond first instability is well understood (see Timoshenko, 1935; Biezeno, 1938; Marguerre, 1938; Fung and Kaplan, 1952; Hoff and Bruce, 1954; Gjelsvik and Bodner, 1962;

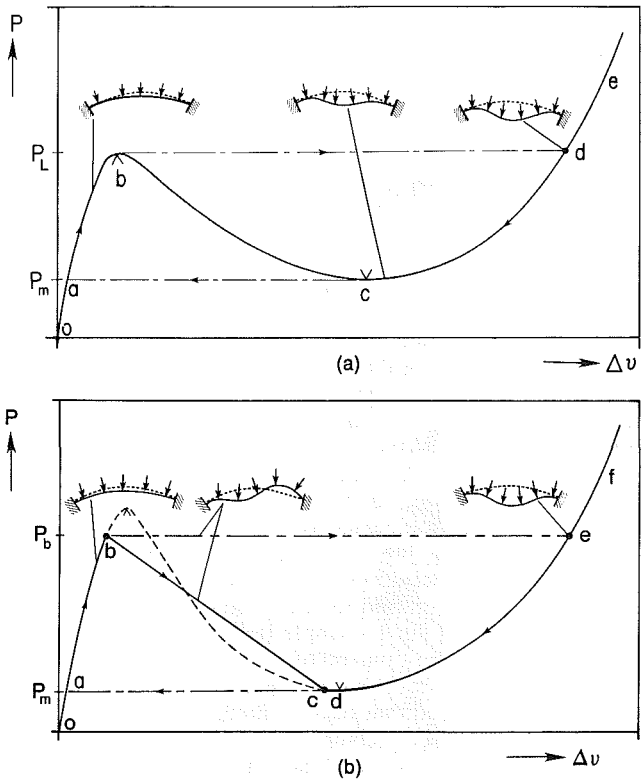

Fig. 1 (*a*) **Pressure-volume change response for arch which buckles symmetrically;** (*b*) **pressure-volume change response for arch which bifurcates into an unsymmetric mode for part of the response**

Contributed by the Applied Mechanics Division of THE AMERICAN SOCIETY OF MECHANICAL ENGINEERS for publication in the ASME JOURNAL OF APPLIED MECHANICS.

Discussion on this paper should be addressed to the Technical Editor, Professor Lewis T. Wheeler, Department of Mechanical Engineering, University of Houston, Houston, TX 77204-4792, and will be accepted until four months after final publication of the paper itself in the ASME JOURNAL OF APPLIED MECHANICS.

Manuscript received by the ASME Applied Mechanics Division, Mar. 8, 1993; final revision, May 24, 1993. Associate Technical Editor: A. K. Noor.

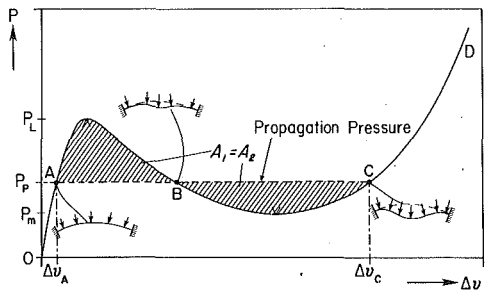

Fig. 2 Maxwell construction for a long shallow panel under uniform pressure

Schreyer and Masur, 1966 and others). Beyond the limit load and under "displacement-controlled" loading, the deformation of the arch in Fig. 1(*a*) grows at a decreasing load, and in the process, the curvature of part of the structure reverses sign. Eventually, further increase in deformation requires membrane stretching. This has a stiffening effect and leads to an upturn in the required load as shown in the figure. If, however, the pressure is prescribed, the structure, upon reaching the limit pressure (P_L), "snaps" from equilibrium point *b* to *d*. Unloading from point *d* to pressure P_m takes place along *dc*. Upon reaching P_m, the structure "snaps" to point *a* on the initial ascending branch. (This snapping back and forth is known as the oil-can effect.)

In the case of the less shallow arch shown in Fig. 1(*b*), the unsymmetric mode of deformation is preferred from point *b* to point *c* on the response. At the bifurcation pressure (P_b), the structure buckles into an unsymmetric mode. In fact, under displacement-controlled loading, the response follows the straight line joining the bifurcation points *b* and *c* (see Schreyer and Masur, 1966). Under pressure-controlled loading, the arch will snap from *b* to *e*. In the process, the unsymmetric deformation yields to a symmetric one, represented by equilibrium point *e*. Again, if the structure is unloaded from *e* to pressure P_m, path *ed* is followed. At *d*, the arch snaps back to point *a* on the prebuckling equilibrium branch. Thus, for prescribed pressure loading, the main difference between the prebuckling response of the two types of arches shown in Fig. 1 is that the maximum pressure reached is P_b rather than P_L.

The preferred mode of behavior is governed by the arch shallowness parameter

$$\lambda = \alpha^2 \frac{R}{t} \tag{1}$$

where 2α is the circular arch span angle, R its radius and t its wall thickness.

The pressure-volume response of both of these types of arches after the first instability has a negative slope. Thus, in the case of a long panel with this same arch as its cross-section, alternate post-buckling branches become available due to the effect of length. Due to the decreasing pressure, localized modes of deformation become energetically preferable to axially uniform collapse. That is, following the onset of the first instability, the deformation ceases to be uniform along the length of the panel. If the pressure is allowed to drop after first buckling (as would occur in volume-controlled pressurization), the buckle can be expected to remain local.

Kyriakides (1993) used a simple experimental apparatus to demonstrate the development of a localized instability in a long, shallow, cylindrical panel loaded by uniform pressure. He also demonstrated that once formed, the local buckle can spread (propagate) at a pressure which is much lower than that required to initiate the instability in a geometrically intact structure. This demonstration experiment will be reviewed below. This work (see also Kyriakides and Arseculeratne, 1993) also showed that the lowest pressure at which such instabilities

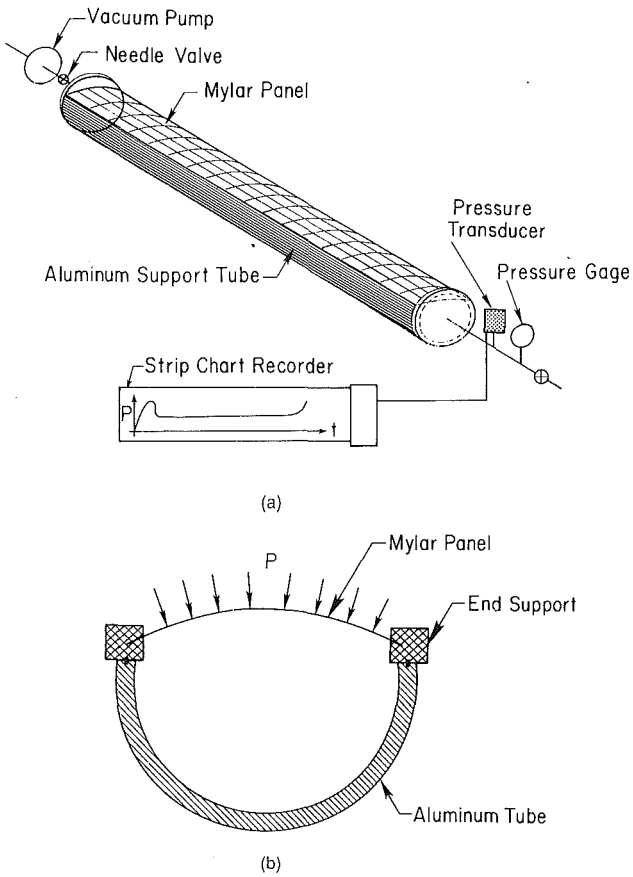

Fig. 3 (*a*) Experimental apparatus used to demonstrate the initiation and propagation of buckles in long panels; (*b*) cross-section of experimental apparatus

will propagate (propagation pressure) can be calculated exactly through an energy balance which utilizes the two-dimensional (axially uniform) response of such panels. This results in the so-called *Maxwell construction* (see Ericksen, 1975; Chater and Hutchinson, 1984; Kyriakides, 1993) shown schematically in Fig. 2. If the two-dimensional response is evaluated using the lowest-order admissible nonlinear kinematics (shallow shell kinematics, see Schreyer and Masur, 1966) the Maxwell construction results in the following closed-form expression for the propagation pressure:

$$P_P = \frac{1}{12} \frac{E}{1-\nu^2} \left(\frac{\pi}{\alpha}\right)^2 \left(\frac{t}{R}\right)^3. \tag{2}$$

In the present work, we use specialized analyses to establish the onset of localized instabilities in long panels and to examine their growth and transformation into propagating buckles. All aspects of the problem are studied in the quasi-static setting. The results are also used to confirm the validity of the propagation pressure yielded by the Maxwell construction.

Experiment

The simple test apparatus used by Kyriakides (1993) to demonstrate the initiation and steady-state propagation of buckles in long panels is shown schematically in Fig. 3. A long shallow panel was formed by bending a strip of thin mylar sheet into the cross-section shown in Fig. 3(*b*). The edges of the mylar strip were positioned and bonded into oblique slits cut into two long metal end support beams. The two end beams were mounted onto a U-shaped aluminum support structure which was made by removing the top of a 4-in. diameter aluminum tube. The arrangement is such that the mylar has a circular arch shape with $R/t = 228$ and an arch parameter $\lambda = 44.7$.

The tubelike structure, whose ends are closed with flanges, has a length of 10 ft (3 m). External pressure loading was applied by evacuating the air inside the closed tube with a vacuum pump. The pressure was monitored with an electrical pressure transducer and was recorded on a strip-chart recorder.

A typical pressure-time history and some of the major features observed during such an experiment are shown schematically in Fig. 4. Pressurization starts at time t_o. Initially, the structure deformed uniformly along its length with a relatively stiff response. For the parameters of this panel, the first instability was unsymmetric buckling (as in Fig. 1(*b*)). Figure 5(*a*) shows the onset of unsymmetric buckling in the panel (we note that this was influenced significantly by geometric imperfections as well as residual stresses present in the demonstration structures used). Soon after the onset of unsymmetric deformation, the structure collapsed dynamically (t_1) and developed a local buckle which was symmetric about the midspan and extended over a length of approximately 7–8 times the arch span (see Fig. 5(*b*)). Under the loading conditions used, the snap-through buckling produced a significant pressure transient. Once formed, the geometry of the local buckle could be frozen by interrupting the evacuation of air from the closed tube (i.e., after t_2). Once the local buckle was fully developed, further propagation of the buckle occurred at a well-defined pressure which was significantly lower than the pressure recorded at the initiation of local collapse. The buckle propagated in both directions until it reached one of the ends. Propagation continued on the other side until the whole panel was collapsed. The rate of propagation of the buckle was controlled by controlling the rate at which the closed system was evacuated. Figure 5(*c*) shows the transition between the buckled and unbuckled sections during such an experiment. Once the buckle reached both ends of the panel (t_4), further deformation required a significant increase in the pressure and was uniform along the length of the structure. The initial maximum pressure recorded is known as *initiation pressure* (P_I) and the pressure at which the collapse propagated is the *propagation pressure* (P_P) of the structure.

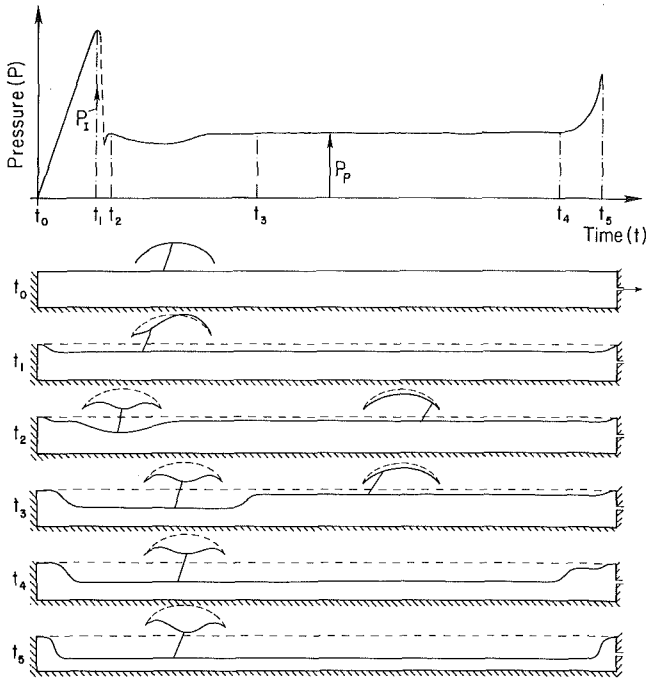

Fig. 4 Schematic representation of the history of an experiment in which a buckle is initiated and propagated in a long panel

Analysis

We consider a circular cylindrical panel of radius R, span angle 2α, thickness t ($\ll R$), and overall length $2L$ subjected to uniform pressure loading (P) over its entire surface as shown in Fig. 6. The panel material is taken to be linearly elastic with Young's modulus E and Poisson's ratio ν. Without loss of generality, the plane $x_1 = 0$ is assumed to be a plane of symmetry. We will consider panels with low values of λ for which deformations remain symmetric about the midspan and panels with higher values of λ which exhibit unsymmetric bifurcation buckling. For symmetric deformations, the plane $x_2 = 0$ is another plane of symmetry and only the darkly shaded portion ($0 \le x \le L$, $0 \le \theta \le \alpha$) of the panel in Fig. 6 is analyzed. For unsymmetric deformations, the problem domain is $0 \le x \le L$, $-\alpha \le \theta \le \alpha$.

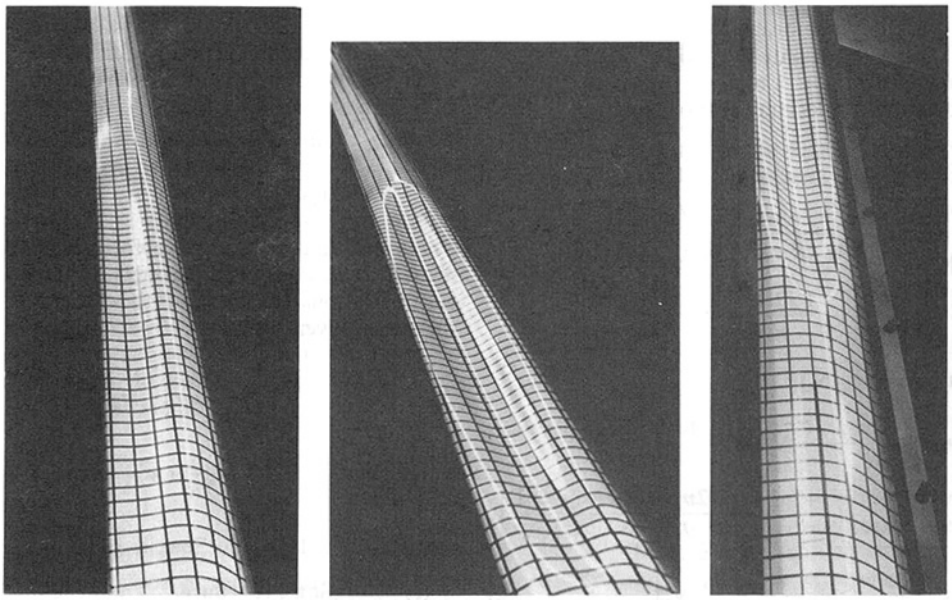

Fig. 5(*a*) Fig. 5(*b*) Fig. 5(*c*)

Fig. 5 Photographs of deformed panel. Fig. 5(*a*) unsymmetric buckle; Fig. 5(*b*) local symmetric buckle; Fig. 5(*c*) transition region between collapsed and uncollapsed portions.

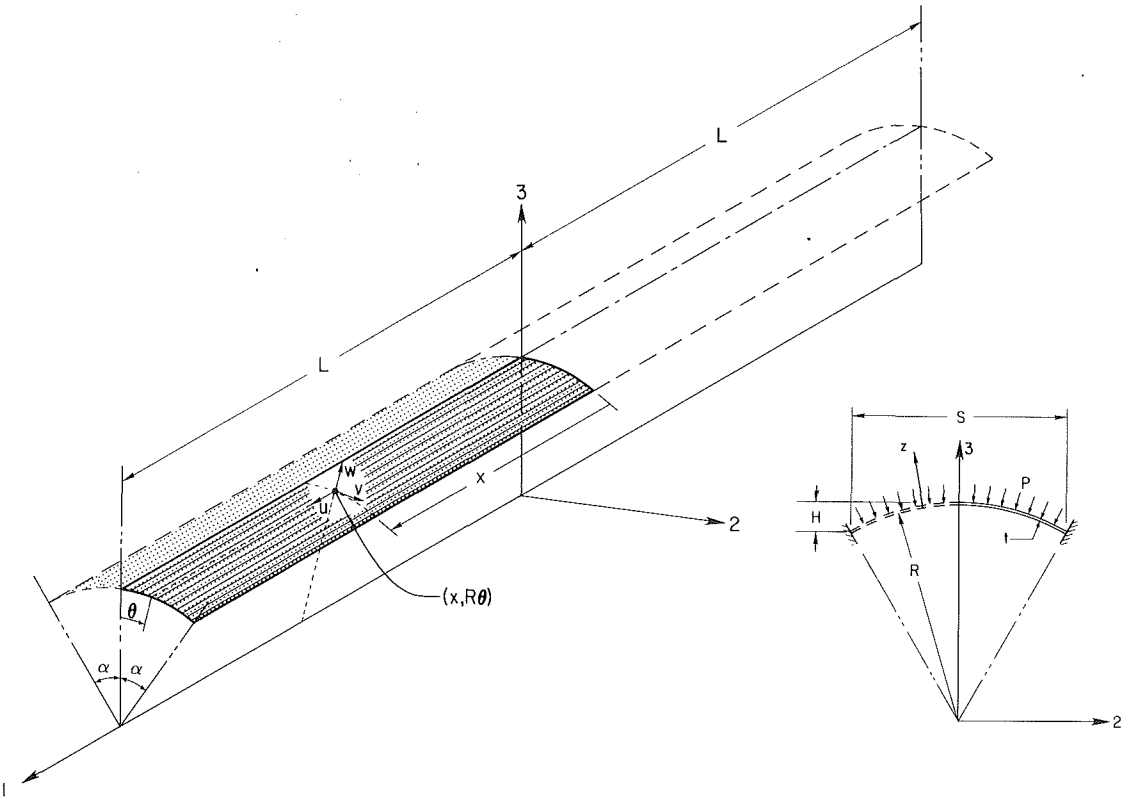

Fig. 6 Geometry of analyzed panel

(a) Kinematics. Sanders (1963) nonlinear shell kinematics with the assumption of small membrane strains are adopted. The particular form of the strain-displacement equations used (specialized for circular cylindrical geometry) was utilized by Dyau and Kyriakides (1993) in their studies of localization of collapse in long metal tubes. Points on the undeformed mid-surface are identified by $(x, R\theta)$, and axial, circumferential, and radial displacements are denoted by u, v, and w, respectively. The strain at any point in the panel is approximated by

$$\epsilon_{\alpha\beta} = (E_{\alpha\beta} + zK_{\alpha\beta})/(A_\alpha A_\beta)^{1/2} \tag{3}$$

where $E_{\alpha\beta}$ and $K_{\alpha\beta}$ are the membrane strains and curvatures, respectively, and z is the coordinate normal to the midsurface (see inset in Fig. 6). Here, $A_1 = 1$ and $A_2 \approx (1 + z/R)$. The strains are related to the displacements through

$$E_{xx} = u_{,x} + \frac{1}{2}[u_{,x}^2 + v_{,x}^2 + w_{,x}^2],$$

$$E_{\theta\theta} = \frac{w + v_{,\theta}}{R} + \frac{1}{2}\left(\frac{u_{,\theta}}{R}\right)^2 + \frac{1}{2}\left(\frac{v_{,\theta} + w}{R}\right)^2 + \frac{1}{2}\left(\frac{w_{,\theta} - v}{R}\right)^2,$$

$$E_{x\theta} = \frac{1}{2}\left[\frac{u_{,\theta}}{R} + v_{,x} + u_{,x}\frac{u_{,\theta}}{R} + v_{,x}\frac{v_{,\theta} + w}{R} + w_{,x}\frac{w_{,\theta} - v}{R}\right],$$

$$K_{xx} = -[u_{,xx}N_x + v_{,xx}N_\theta + w_{,xx}N_z],$$

$$K_{\theta\theta} = -\left[\frac{u_{,\theta\theta}}{R^2}N_x + \frac{v_{,\theta\theta} + 2w_{,\theta} - v}{R^2}N_\theta + \frac{w_{,\theta\theta} - 2v_{,\theta} - w - R}{R^2}N_z + \frac{1}{R}\right],$$

$$K_{x\theta} = -\left[\frac{u_{,x\theta}}{R}N_x + \frac{v_{,x\theta} + w_{,x}}{R}N_\theta + \frac{w_{,x\theta} - v_{,x}}{R}N_z\right], \tag{4}$$

where N_i are the components of the normal to the deformed panel mid-surface given by

$$N_x \cong v_{,x}\frac{w_{,\theta} - v}{R} - w_{,x}\frac{w + v_{,\theta}}{R} - w_{,x},$$

$$N_\theta \cong w_{,x}\frac{u_{,\theta}}{R} - u_{,x}\frac{w_{,\theta} - v}{R} - \frac{w_{,\theta} - v}{R},$$

$$N_z \cong 1 + u_{,x} + \frac{w + v_{,\theta}}{R} + u_{,x}\frac{w + v_{,\theta}}{R} - v_{,x}\frac{u_{,\theta}}{R}. \tag{5}$$

(b) Principle of Virtual Work. Equilibrium of the structure was enforced through the principle of virtual work (PVW) which for uniform, lateral pressure loading may be expressed as follows:

$$\int_0^L \int_{0,(-\alpha)}^{\alpha} [N_{\alpha\beta}\delta E_{\alpha\beta} + M_{\alpha\beta}\delta K_{\alpha\beta}]Rd\theta dx = -P\delta\Delta v^\dagger \tag{6}$$

where $N_{\alpha\beta}$ and $M_{\alpha\beta}$ are the force and moment intensities, related to $E_{\alpha\beta}$ and $K_{\alpha\beta}$ through the usual isotropic linearly elastic relationships, and Δv is the change in volume underneath the panel, given by

$$\Delta v = \int_0^L \int_{0,(-\alpha)}^{\alpha} \left[w + \frac{1}{2}(wu_{,x} - w_{,x}u) + \frac{1}{2R}(w^2 + wv_{,\theta} - w_{,\theta}v + v^2)\right]Rd\theta dx \tag{7}$$

(see Pearson, 1956 and Sewell, 1965).

(c) Solution Procedure. The structure was discretized using the following expansions for the displacements:

†The limits of integration in parentheses are used in the unsymmetric case.

$$u = R\sum_{m=1}^{M}\sin\frac{m\pi x}{L}\left\{\sum_{n=1}^{N_s}c_{mn}\left[\cos\left(\frac{2n-1}{2}\frac{\pi\theta}{\alpha}\right)\right]+\sum_{n=1}^{N_a}g_{mn}\left[\sin\frac{n\pi\theta}{\alpha}\right]\right\},$$

$$v = R\sum_{m=1}^{M}\cos\frac{(m-1)\pi x}{L}\left\{\sum_{n=1}^{N_s}b_{mn}\left[\sin\frac{n\pi\theta}{\alpha}\right]+\sum_{n=1}^{N_a}h_{mn}\left[\frac{\alpha}{\mu_n}\cos\left(\mu_n\frac{\theta}{\alpha}\right)+\frac{\theta^2}{2\alpha}\mu_n\cos\mu_n-\alpha\left(\frac{\mu_n}{2}+\frac{1}{\mu_n}\right)\cos\mu_n\right]\right\},$$

$$w = R\sum_{m=1}^{M}\cos\frac{(m-1)\pi x}{L}\left\{\sum_{n=1}^{N_s}a_{mn}\frac{1}{2}\left[(-1)^{n+1}+\cos\frac{n\pi\theta}{\alpha}\right]+\sum_{n=1}^{N_a}f_{mn}\left[\sin\left(\mu_n\frac{\theta}{\alpha}\right)-\frac{\theta}{\alpha}\mu_n\cos\mu_n\right]\right\} \quad (8)$$

where μ_n are the positive roots of $\tan\mu_n = \mu_n$. These functions satisfy fixed conditions along the boundaries $\theta = \pm\alpha$ and exhibit symmetry in x. In addition, $w_{,x}$ vanishes at the boundaries $x = \pm L$. The first summation in each displacement component models deformation symmetric in θ, whereas the second summation models deformation antisymmetric in θ. Thus, for the symmetric case, f_{mn}, g_{mn}, and h_{mn} are set to zero. The number of axial half waves (M) used was typically 2–3 times the L/S ratio for a given geometry, and the number of circumferential half waves (both N_s and N_a) was taken to be 6. These values were determined adequate by convergence studies. Integration was performed by Gaussian quadrature. The panel was loaded incrementally by prescribing either the displacement $w(0, 0)$ or the change in volume underneath the panel, Δv, depending on the current nature of the response. The nonlinear equations resulting from Eqs. (3)–(8) were solved using the Newton-Raphson method.

Results and Discussion

Due to the obvious differences in the ways instabilities are initiated and localize for panels with different values of λ, we will discuss separately the behavior of panels with low enough values of λ to deform symmetrically about the midspan and that of panels which deform unsymmetrically. The panels analyzed have $R/t = 480$; various values of λ are achieved by varying the angle α.

(a) Symmetric Initiation and Propagation of Collapse. The features of the response of panels which buckle and collapse symmetrically about the midspan will be discussed by way of an example with $\lambda = 5.6$. For this case, the primary response (axially uniform and symmetric) exhibits bifurcations into unsymmetric modes on the descending portion following the limit load. The events that we will discuss precede these instabilities and thus their effect is irrelevant to our discussion. The calculated primary pressure-volume change response of such a panel with a length of 20 spans is shown in Fig. 7 where the following normalizations are adopted:

$$\bar{P} = \frac{P}{\frac{E}{12(1-\nu^2)}\left(\frac{\pi}{\alpha}\right)^2\left(\frac{t}{R}\right)^3} \quad \text{and} \quad \Delta\bar{v} = -\frac{1}{\alpha^3}\frac{\Delta v}{R^2 L}. \quad (9)$$

This response is stable up to the limit pressure (identified by "^"). Due to the negative slope of the primary response beyond the limit load, it is easy to visualize that localized modes of collapse may be preferable to axially uniform collapse. The unstable nature of this part of the response can indeed be easily verified by conducting a linearized bifurcation check. This was done as summarized in the Appendix and involved the following buckling modes which are symmetric about the midlength of the panel:

$$\tilde{u} = \sin\frac{m\pi x}{L}\sum_{n=1}^{N}B_n\cos\left(\frac{2n-1}{2}\frac{\pi\theta}{\alpha}\right), \quad m = 1, 2, 3\ldots$$

$$\tilde{v} = \cos\frac{m\pi x}{L}\sum_{n=1}^{N}C_n\sin\frac{n\pi\theta}{\alpha},$$

$$\tilde{w} = \cos\frac{m\pi x}{L}\sum_{n=1}^{N}A_n\left[(-1)^{n+1}+\cos\frac{n\pi\theta}{\alpha}\right]. \quad (10)$$

The first bifurcation point identified corresponds to $m = 1$ and occurs at $\Delta\bar{v} = 0.1430$, very soon after the limit pressure at $\Delta\bar{v} = 0.1426$. Subsequent bifurcation points, with progressively higher values of m, occur at increasingly higher values of $\Delta\bar{v}$. The first four bifurcation points are identified with Roman numerals in the inset of Fig. 7.

The onset of instability is affected by the length of the panel. This is demonstrated in Fig. 8 which shows expanded views

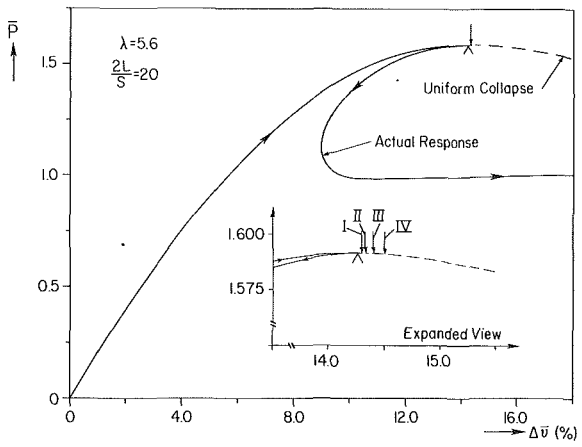

Fig. 7 Calculated pressure-volume change response for $\lambda = 5.6$

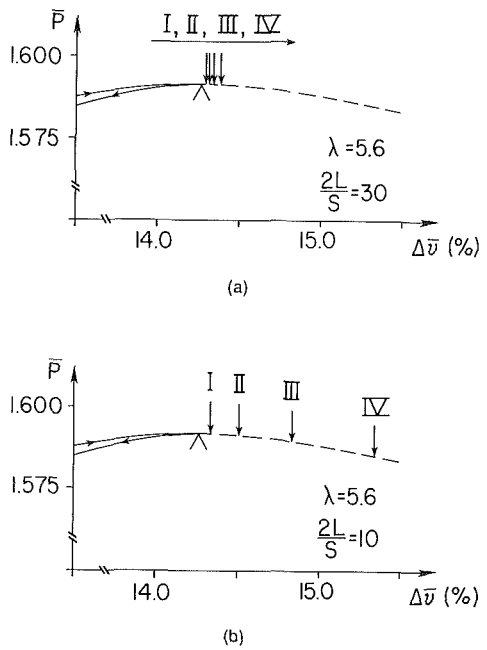

Fig. 8 Expanded view of critical region of pressure-volume change response for $\lambda = 5.6$; (*a*) 2L = 30S; (*b*) 2L = 10S

of the response in the region of the limit load for two additional panels with lengths of $2L = 30S$ and $10S$. Comparing the positions of the bifurcation points of the three cases, we observe that decreasing the length of the panel has the effect of delaying the onset of the first bifurcation point and increases the distance between subsequent bifurcation points. Conversely, for a very long panel, the limit load is an accumulation point. Thus, the limit load can be viewed as the critical point of the primary response.

This type of behavior has been observed before in other problems characterized by natural limit load instabilities such as necking of bars under uniaxial tension (Hutchinson and Miles, 1974) and bulging of internally pressurized tubes (Kyriakides and Chang, 1991).

The actual response of the structure following the first instability is also included in Fig. 7. It can be seen that the response beyond the bifurcation point reverses direction, that is, both the volume change and the pressure decrease, forming a cusp-like shape. A more complete view of the actual postbuckling response is shown in Fig. 9 which includes a sequence of deformed configurations of the line $\theta = 0$. The configurations are identified on the $P - \Delta v$ response by numbered points. On the ascending part of the response (⓪-③) the panel deforms uniformly along the length. The line $\theta = 0$ is seen in Fig. 9(*b*) to remain straight as it deflects downward. At point ③ the volume under the arch has been reduced significantly. Beyond point ③, a localized mode of deformation appears. In the case shown, the region of the panel around midlength is seen to experience local collapse while the overall pressure required for equilibrium decreases. Configurations ④ to ⑨ clearly show the growth of local collapse. Full views of some of the deformed configurations identified in Fig. 9 are presented in Fig. 10 (rendered from the solution

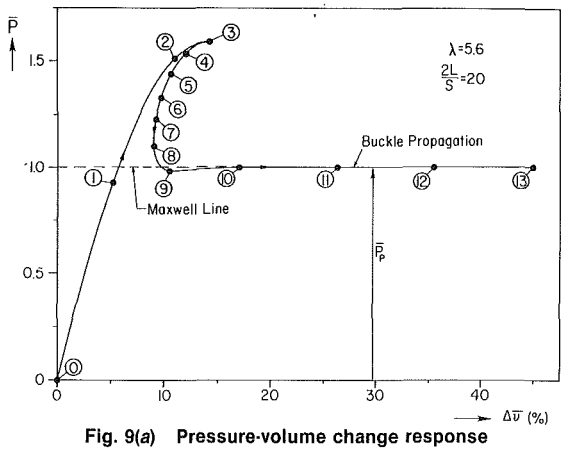

Fig. 9(*a*) Pressure-volume change response

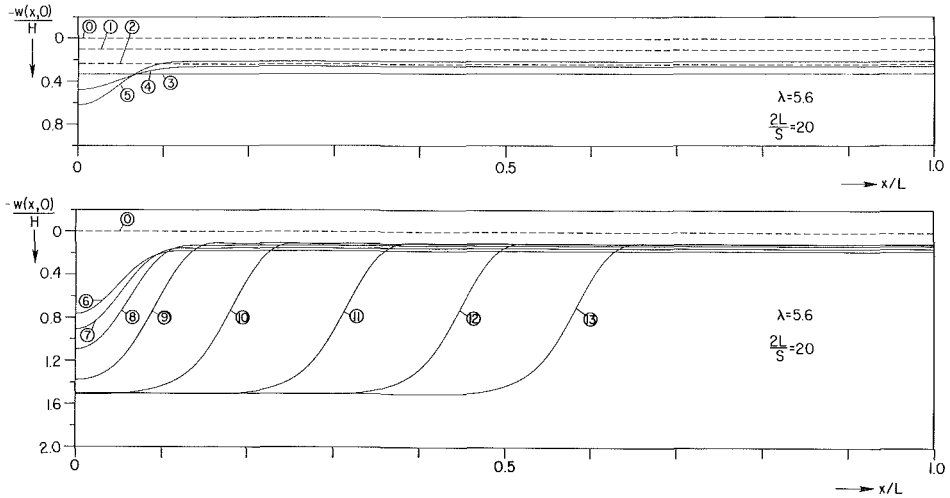

Fig. 9(*b*) Deformed configurations of generator $\theta = 0$

Fig. 9 Panel analysis: $\lambda = 5.6$, $2L = 20S$

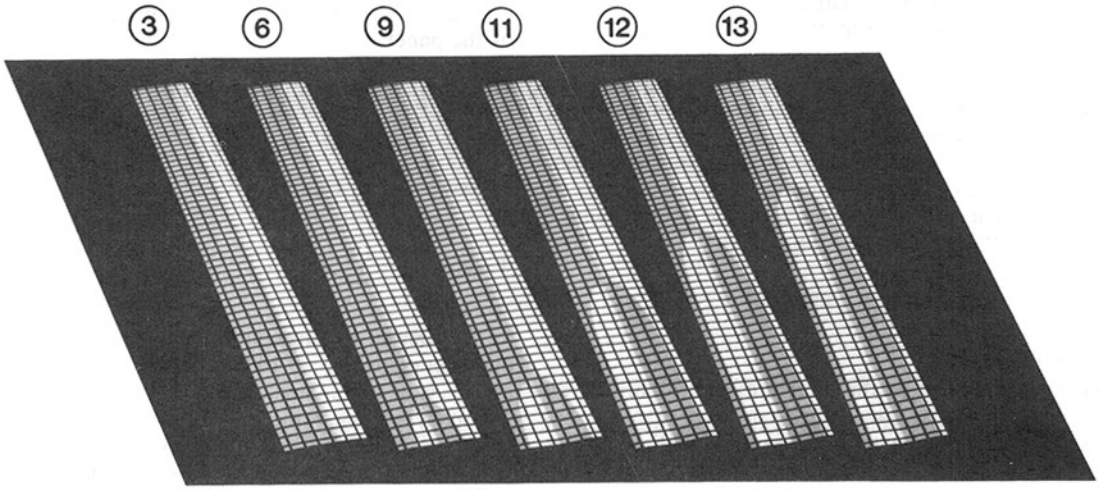

Fig. 10 Sequence of calculated configurations for panel of Fig. 9 showing symmetric initiation and propagation of collapse

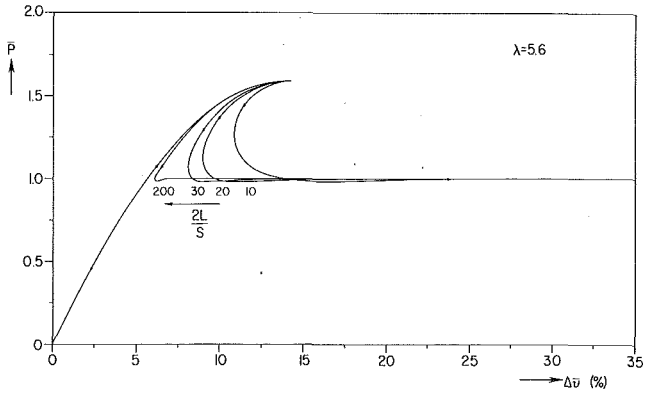

Fig. 11 Calculated pressure-volume change responses for λ = 5.6 and various panel lengths

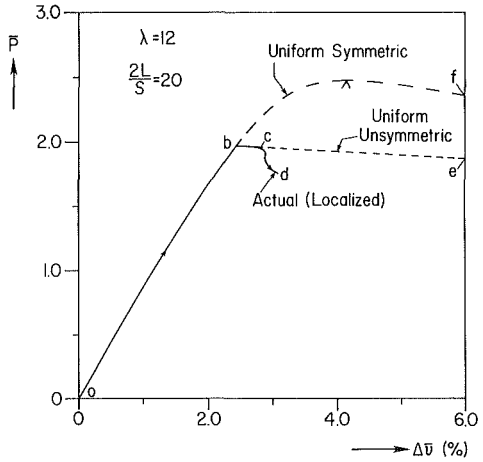

Fig. 12 Calculated pressure-volume change response for λ = 12

using the *SunVision* image processing system). It is interesting to observe that away from the collapsing region the panel deforms uniformly, unloading (as a result of the decreasing pressure) along a path (③-⓪) that corresponds to the one followed during loading. Thus, away from the localized collapse, the line $\theta = 0$ is seen to move upward, indicating an increase in the volume under this region of the panel.

This dichotomy in behavior between the collapsing section and the remainder of the structure is responsible for the cusp-like nature of the overall response shown in Figs. 7 and 9. For longer panels, like the case analyzed, the increase in volume under the section which is unloading is much larger than the decrease in volume under the collapsing section. This results in the net volume change shown in the figures.

The localization process is eventually arrested by membrane tension in the most collapsed region. With this region stabilized, further collapse will occur in adjacent less deformed sections until they become stabilized in turn. Thus, beyond ⑨, the localization of collapse gives way to propagation of collapse along the panel. By configuration ⑩, this propagation reaches a steady state in which a well-defined transition region, or front (actually one on either side of the collapsed region) has formed, joining the collapsed and uncollapsed parts of the structure. Thus, further decrease of the volume under the panel results in propagation (⑩-⑬) of the front which progressively engulfs uncollapsed sections and leaves collapsed sections in its wake. The value of pressure which accommodates this steady-state propagation corresponds exactly to that predicted by the Maxwell construction discussed in the introduction and given approximately by (2).

The propagation of the front will continue until the whole length of the panel is collapsed as discussed in the experimental section. In the case shown in the figure, the calculation was interrupted at configuration ⑬.

As in other structures exhibiting localization, the overall length of the panel affects the initial part of the calculated response (see Kyriakides and Chang, 1991). Figure 11 shows a comparison of the $P - \Delta v$ responses of panels with the same cross-section for lengths of 10, 20, 30, and 200 spans. The size of the cusp which follows the limit load is seen to grow with the length of the panel. In fact, for a very long panel, the cusp portion of the response follows (in reverse) almost the same path as that followed in the initial uniform part of the response. The reason for this is that for such a long panel the volume decrease in the locally collapsing section is small compared to the volume change in the rest of the panel which is experiencing unloading. Quite clearly, in volume-controlled pressurization of such panels, the cusp-like parts of the calculated response would not be realized. Instead, upon reaching the limit load, the response would experience a dynamic drop from the limit pressure to the propagation pressure.

(b) Unsymmetric Initiation and Symmetric Propagation of Collapse. The characteristics of the response of panels which bifurcate from the primary symmetric response into an unsymmetric mode before the natural limit load is achieved will be discussed through an example with $\lambda = 12$ and a length of 20 spans. The calculated response for this geometry, in the neighborhood of the first instability, is shown in Fig. 12. Initially, (path *ob*) the panel deformation is uniform along the length and symmetric about the midspan. The bifurcation into unsymmetric deformation occurs at *b* and corresponds to $(\bar{P}, \Delta\bar{v}) = (1.970, 0.0244)$. The bifurcation mode is axially uniform and is given by

$$\tilde{w} = A\left[\sin\left(\mu\frac{\theta}{\alpha}\right) - \left(\mu\frac{\theta}{\alpha}\right)\cos\mu\right] \tag{11}$$

where μ is the lowest positive root of $\tan\mu = \mu$ (see Schreyer and Masur, 1966). If the unsymmetric postbifurcation deformation were constrained to be axially uniform, the calculated response would follow path *be* in the figure. This path has a negative slope and rejoins the primary response as shown schematically in Fig. 1(*b*). Due to this negative slope, we can again expect localized modes to be preferable to continued axially uniform collapse. Indeed, *bcd* represents the response calculated when the unsymmetric deformation is allowed to localize. Due to the finite length of the panel analyzed, significant departure from path *be* is delayed until point *c*. Again, localized deformation is accompanied by a rather abrupt drop in pressure, but for this length, $\Delta\bar{v}$ remains monotonically increasing.

In the interest of making the problem more realistic, we consider the same panel geometry but introduce a small initial imperfection corresponding to the unsymmetric buckling mode (11). The calculated $P - \Delta v$ response is shown in Fig. 13 together with sets of cross-section configurations for locations A and B which are identified in the inset. Full views of the deformed configurations corresponding to points ① to ⑥ on the response are shown in Fig. 14. The panel initially deforms in a primary symmetric fashion (⓪-①). In the neighborhood of the unsymmetric bifurcation of the perfect problem, the imperfection activates axially uniform, unsymmetric deformations clearly shown in configurations ② in Fig. 13 (note also the off-center position of the shade boundary in Fig. 14).

The response develops a limit load at ② beyond which the deformation starts to localize. In the process, the deformation of a section of the panel at midlength experiences continued growth at a dropping overall pressure, while the remainder of the panel unloads. This difference is clearly illustrated in Fig. 13 by comparing the cross-section configurations of locations A and B corresponding to ③ (see also Fig. 14). As localization continues, the shape of the most deformed cross-section is seen to become progressively more symmetric. Local deformation

is eventually arrested by membrane tension, and the collapse, which by this time has become symmetric, starts to propagate along the panel. For long panels, the propagation of the collapse can occur in a steady-state fashion and has essentially the same features as those of the symmetric case discussed in Section (a). The propagation pressure again corresponds to that predicted by the Maxwell construction ($\bar{P}_P = 1.0046$).

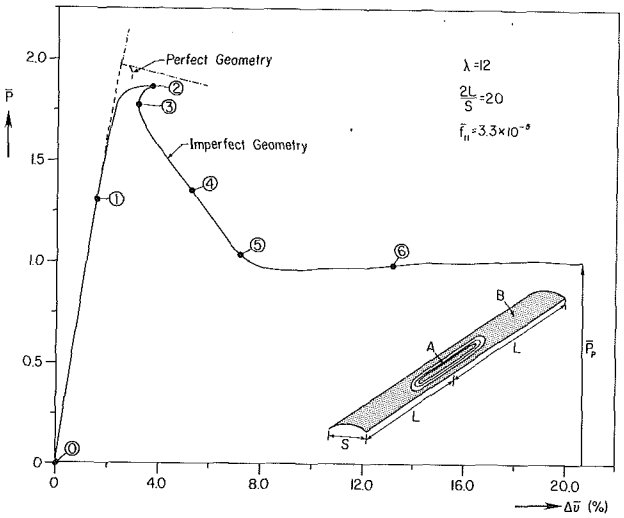

Fig. 13(*a*) Pressure-volume change response

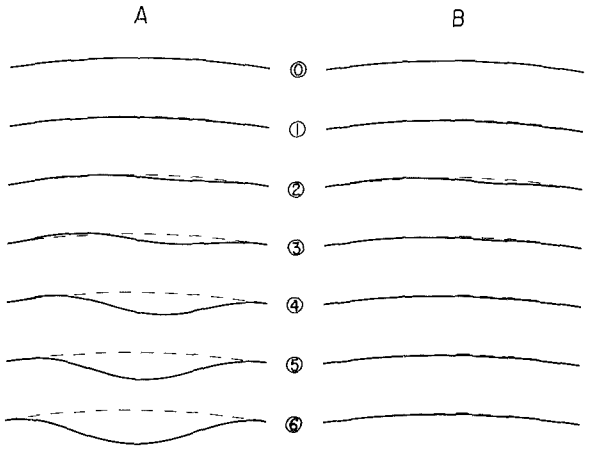

Fig. 13(*b*) Sequence of cross-section configurations at A and B (displacements amplified 2 ×)

Fig. 13 Panel analysis: λ = 12, 2*L* = 20*S*, with uniform unsymmetric initial imperfection

Summary and Conclusions

It has been demonstrated that, in addition to the classical limit load and bifurcation buckling instabilities, long panels can also develop propagating buckles. Once initiated, such buckles will propagate as long as the pressure is higher than the propagation pressure. In general, the propagation pressure is significantly lower than the classical critical pressures associated with the perfect structure.

The objective of the present work was to demonstrate that in such structures the classical instabilities trigger localization of collapse and the initiation of propagating buckles. In the case of panels with lower values of the arch parameter λ, the critical instability of geometrically perfect panels is the limit pressure of the primary symmetric response. In has been shown that following the load maximum the symmetric deformation localizes to a section a few panel spans long, while the remainder of the panel unloads uniformly. The pressure-volume change response follows a cusp-like shape until the localized collapse is arrested by membrane tension. Following this, and under prescribed volume loading, the collapse can propagate along the length at the propagation pressure.

In the case of panels with higher values of λ, the primary symmetric response is interrupted by a bifurcation into an axially uniform, unsymmetric mode before the limit pressure is reached. It has been shown that soon after its onset, this mode of deformation also localizes to a section a few panel spans long. As the deformation progresses, the unsymmetric local deformation gradually yields to a symmetric one. Local deformation is eventually arrested by membrane tension and the collapse can then propagate down the panel.

The propagation pressure of elastic panels exhibiting either type of behavior can be calculated exactly by the Maxwell construction and is given approximately by Eq. (2).

The main requirements for the existence of the type of behavior described are that the structure have a local up-down-up load-deformation response, as those shown in Fig. 1, and that it be long (see Kyriakides, 1993). Thus, long panels with other arch geometries, boundary conditions and load distributions can be expected to exhibit similar localized and propagating instabilities.

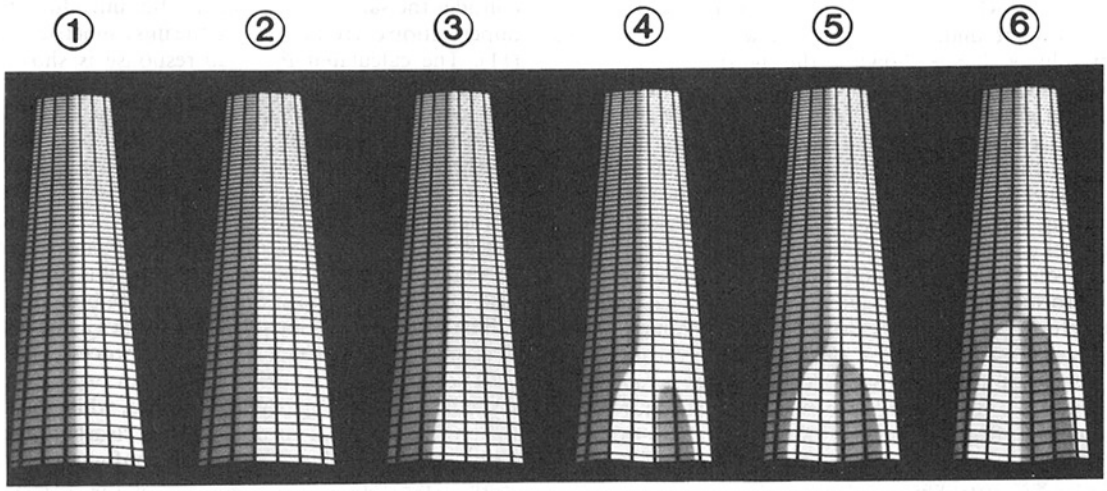

Fig. 14 Sequence of calculated configurations for panel of Fig. 13 showing unsymmetric initiation of collapse followed by symmetric propagation

Acknowledgment

The work was supported in part by the Office of Naval Research through grant N-00014-91-J-1103 and by the University of Texas at Austin.

References

Biezeno, C. B., 1938, "Das Durchschlagen Eines Schwach Gekrummten Stabes," *Zeitschrift fur Angewandte Mathematik und Mechanik*, Vol. 18, pp. 21-30.

Chater, E., and Hutchinson, J. W., 1984, "On the Propagation of Bulges and Buckles," ASME JOURNAL OF APPLIED MECHANICS, Vol. 51, pp. 269-277.

Dyau, J. Y., and Kyriakides, S., 1993, "On the Localization of Collapse in Cylindrical Shells Under External Pressure," *International Journal of Solids and Structures*, Vol. 30, pp. 463-482.

Ericksen, J. L., 1975, "Equilibrium of Bars," *Journal of Elasticity*, Vol. 5, pp. 191-201.

Fung, Y. C., and Kaplan, A., 1952, "Buckling of Low Arches or Curved Beams of Small Curvature," *NACA TN* 2840.

Gjelsvik, A., and Bodner, S. R., 1962, "The Energy Criterion and Snap Buckling of Arches," *ASCE Journal of the Engineering Mechanics Division*, Vol. 88, No. 4, pp. 87-134.

Hoff, N. J., and Bruce, V. G., 1954, "Dynamic Analysis of the Buckling of Laterally Loaded Flat Arches," *Journal of Mathematics and Physics*, Vol. 32, pp. 276-288.

Hutchinson, J. W., and Miles, J. P., 1974, "Bifurcation Analysis of the Onset of Necking in an Elastic/Plastic Cylinder Under Uniaxial Tension," *Journal of the Mechanics and Physics of Solids*, Vol. 22, pp. 61-71.

Kyriakides, S., 1993, "Propagating Instabilities in Structures," *Advances in Applied Mechanics*, Vol. 30, J. W. Hutchinson and T. Y. Wu, eds., Academic Press, Boston, MA, pp. 67-189.

Kyriakides, S., and Arseculeratne, R., 1993, "Propagating Instabilities in Long Shallow Panels," *ASCE Journal of Engineering Mechanics*, Vol. 119, No. 3, pp. 570-583.

Kyriakides, S., and Chang, Y.-C., 1991, "The Initiation and Propagation of a Localized Instability in an Inflated Elastic Tube," *International Journal of Solids and Structures*, Vol. 27, pp. 1085-1111.

Marguerre, K., 1938, "Uber die Anwendung der Energetischen Methode auf Stabilitatsprobleme," DVL 252-262; also *NACA TM* 1138, 1947.

Pearson, C. E., 1956, "General Theory of Elastic Stability," *Quarterly of Applied Mathematics*, Vol. 14, pp. 133-144.

Sanders, J. L., 1963, "Nonlinear Theories for Thin Shells," *Quarterly of Applied Mathematics*, Vol. 21, pp. 21-63.

Sewell, M. J., 1965, "On the Calculation of Potential Functions Defined on Curved Boundaries," *Proceedings of the Royal Society of London*, Vol. A286, pp. 402-411.

Schreyer, H. L., and Masur, E. F., 1966, "Buckling of Shallow Arches," *ASCE Journal of the Engineering Mechanics Division*, Vol. 92, pp. 1-19.

Timoshenko, S., 1935, "Buckling of Flat Curved Bars and Slightly Curved Plates," ASME JOURNAL OF APPLIED MECHANICS, Vol. 2, pp. A17-A27.

APPENDIX

Bifurcation Into Axially Nonuniform Shape

At any calculated equilibrium state on the primary response, (symmetric, axially uniform) the second variation ($\delta^2 V$) of the potential energy associated with the bifurcation modes (10) may be evaluated. Vanishing of $\delta^2 V$ indicates loss of stability of the uniform configuration. We define $\tilde{\mathbf{q}}$ as

$$\tilde{\mathbf{q}} = [A_1, A_2, \ldots, A_N, B_1, B_2, \ldots, B_N, C_1, C_2, \ldots, C_N]^T \tag{A1}$$

where A_i, B_i and C_i are the mode coefficients in (10). The second variation of the potential energy of the panel may then be expressed as

$$\begin{aligned}\delta^2 V = \int_0^L \int_0^\alpha \Big\{ & \tilde{N}_{\alpha\beta,i}\tilde{E}_{\alpha\beta,j} + \tilde{M}_{\alpha\beta,i}\tilde{K}_{\alpha\beta,j} \\ & + N^0_{xx}(\tilde{\phi}_{1,i}\tilde{\phi}_{1,j} + \tilde{\phi}_{,i}\tilde{\phi}_{,j}) + N^0_{\theta\theta}(\tilde{\phi}_{2,i}\tilde{\phi}_{2,j} + \tilde{\phi}_{,i}\tilde{\phi}_{,j}) \\ & + P\Big[(\tilde{u}_{,xi}\tilde{w}_{,j} - \tilde{u}_{,i}\tilde{w}_{,xj}) + \frac{1}{R}(\tilde{v}_{,i}\tilde{v}_{,j} + \tilde{v}_{,\theta i}\tilde{w}_{,j} \\ & - \tilde{v}_{,i}\tilde{w}_{,\theta j} + \tilde{w}_{,i}\tilde{w}_{,j}) \Big] \Big\} R\,d\theta\,dx\,\tilde{q}_i\tilde{q}_j \end{aligned} \tag{A2}$$

where $(\ )^0$ corresponds to the values in the primary equilibrium state, and derivatives with respect to $\tilde{q}_i$ are denoted by $(\ )_{,i}$. Implicit in the derivation of Eq. (A2) are Sanders' (1963) nonlinear strain-displacement relations for moderate rotations. These relationships, when linearized, yield

$$\begin{aligned} \tilde{E}_{xx} &= \tilde{u}_{,x} + \phi^0_1\tilde{\phi}_1 + \phi^0\tilde{\phi}, \\ \tilde{E}_{\theta\theta} &= \frac{1}{R}(\tilde{v}_{,\theta} + \tilde{w}) + \phi^0_2\tilde{\phi}_2 + \phi^0\tilde{\phi}, \\ \tilde{E}_{x\theta} &= \frac{1}{2}\left[\left(\tilde{v}_{,x} + \frac{1}{R}\tilde{u}_{,\theta} \right) + \phi^0_1\tilde{\phi}_2 + \phi^0_2\tilde{\phi}_1 \right], \\ \tilde{K}_{xx} &= \tilde{\phi}_{1,x}, \\ \tilde{K}_{\theta\theta} &= \frac{1}{R}\tilde{\phi}_{2,\theta}, \\ \tilde{K}_{x\theta} &= \frac{1}{2}\left[\frac{1}{R}\tilde{\phi}_{1,\theta} + \tilde{\phi}_{2,x} + \frac{1}{R}\tilde{\phi} \right] \end{aligned} \tag{A3}$$

where

$$\tilde{\phi}_1 = -\tilde{w}_{,x}, \quad \tilde{\phi}_2 = \frac{1}{R}(\tilde{v} - \tilde{w}_{,\theta}) \text{ and } \tilde{\phi} = \frac{1}{2}\left(\tilde{v}_{,x} - \frac{1}{R}\tilde{u}_{,\theta} \right).$$

Equation (A2) then reduces to the quadratic form $\delta^2 V = \tilde{\mathbf{q}}^T\mathbf{H}\tilde{\mathbf{q}}$. Thus, loss of stability of the primary response is indicated by the vanishing of the determinant of $\mathbf{H}$.